Engineering Structures 183 (2019) 18–29

Contents lists available at ScienceDirect

Engineering Structures

journal homepage: www.elsevier.com/locate/engstruct

RC arch bridge seismic performance evaluation by sectional N-M interaction and coupling effect of brace beams

Kailai Deng[a,b], Guihao Yan[a], Haipeng Yang[a], Canhui Zhao[a,*]

[a] Department of Bridge Engineering, Southwest Jiaotong University, Chengdu 610031, China
[b] Key Laboratory of High-speed Railway Engineering, Ministry of Education, Southwest Jiaotong University, Chengdu 610031, China

ARTICLE INFO

Keywords:
RC arch bridge
Seismic performance
Nonlinear dynamic analysis
N-M interaction
Brace beam
Coupling ratio

ABSTRACT

Reinforced concrete (RC) arch bridges usually sustain remarkable damage from strong earthquakes. To comprehensively investigate the seismic performance of an RC arch bridge, a benchmark RC arch bridge was modeled with the ABAQUS software, and the seismic performance in the longitudinal and lateral directions was determined at different earthquake intensities. In this paper, the seismic responses, i.e., the mid-span drifts, plasticity development, and N-M interactions at the springing, etc., are discussed. The sectional safety factor is proposed to quantitatively describe the damage degree of the springing section under longitudinal excitation. According to the results, this factor successfully indicated the damage status at the springing, and was consistent with the strain development and the N-M interactions. With regard to the lateral excitation, the current design did not consider the contribution from the brace beams. The coupling ratio (*CR*) is proposed to quantitatively calculate the coupling effect on the two arch ribs from the brace beams. Different *CR*s were tested to enhance the lateral seismic performance. Finally, the recommended *CR* was derived.

1. Introduction

An arch bridge is an effective structure to make full use of the high compressive strength of concrete and masonry material by transferring the gravitational load into the axial force in the main arch [6]. With the development of materials and construction techniques, the amount and scale of arch bridges increased remarkably. However, reinforced concrete (RC) arch bridges are built to cross deep valleys in mountainous areas and are exposed to severe earthquake risk. During the 2008 Wenchuan earthquake in China, more than 100 arch bridges incurred different degrees of damages, with several bridges collapsing completely [7,4,15]. Moreover, extremes were observed in the earthquake damages to RC arch bridges. In other words, serious damage and the complete absence of damage were quite common in the RC arch rib, while instances of moderate damage were rare. The rehabilitation of damaged RC arch bridge was time-consuming and costly [12]. The earthquake hazards attributed to RC arch bridges are still alarming, and a deep investigation into the damage mechanism of the RC arch bridge is needed.

Alvarez et al. [1] evaluated the seismic performance of an RC arch bridge by using numerical models with plastic hinges in the SAP2000 software, and the seismic performance was indicated by the evolution of plasticity in critical sections. The plastic hinge models were usually generated under a constant axial force, and no deterioration at the springing was considered. However, the axial force in the arch rib was not constant during the earthquake. Zanardo et al. [16] conducted the seismic performance evaluation of the short span concrete arch bridge, which revealed that the axial force of the springing was significantly affected by the vertical components of the ground motions. Under a fluctuating axial force, the sectional plastic hinge model could not deliver the actual seismic behavior of the arch bridge. During an earthquake, a 40% increase in the axial force can be obtained, and may lead to a significant decrease in the rotation capacity of the springing [13]. Moreover, the coupled axial force and moment effect should be considered when dealing with a large axial force.

On the other hand, the brace beam between the arch ribs exerts a significant influence on the lateral dynamic characteristics of the RC arch bridges. With regard to design, the brace beams are simply used to guarantee the stability of the arch ribs, but their restraining effect on the arch rib under a lateral earthquake is not considered. The coupling effect induced by the brace beams contributes to the lateral resistance, particularly under strong lateral excitation [11]. The brace beams and arch ribs constitute a space frame structure, and the brace beams sustain a shear force and moment under lateral excitation. According to Lu et al. [8] and Usami et al. [14], employing the energy dissipation brace in the tie frame between the main arch ribs is effective in reducing the

* Corresponding author.
E-mail address: zch2887@163.com (C. Zhao).

https://doi.org/10.1016/j.engstruct.2019.01.013
Received 2 May 2018; Received in revised form 31 December 2018; Accepted 3 January 2019
0141-0296/ © 2019 Published by Elsevier Ltd.

Nomenclature

CR	coupling ratio
C_{30}	concrete with the cubic compressive strength of 30 MPa
DBE	design-based earthquake
F_y	yielding connector of the connector
GM	ground motion
HRB	hot rolled ribbed steel bar
K_0	initial shear stiffness of the connector
l_{1i}	distance between the i^{th} loading point and initial point
l_{2i}	distance between the i^{th} intersection point and initial point
l	distance between the two arch ribs.
MCE	maximum considered earthquake
$M_{S1(2)}$	sectional moment of each arch rib at springing
$M_{S1(2)}$	sectional moment of each arch rib at mid-span
M_{sp}	yielding section moment of the mid-span and springing section
m_i	sectional moment of the i^{th} brace beam
$N_{1(2)}$	axial force of each arch ribs
OM	overall sectional moment of the half main arch ring
PGA	peak ground motion acceleration
RC	reinforced concrete
VRE	very rare earthquake
w	width of the arch rib
σ_{max}	stress peak value in history
ε_{max}	strain peak value in history
ε_y	yelding strain of the rebar
ε_c	strain at peak strength of concrete
ε_u	strain at 20% of peak strength of concrete
η	sectional safety factor

seismic response of the arch bridge. To this end, the mechanical performance of the brace beams, i.e., the stiffness, strength and ductility, is important to the lateral seismic performance of arch bridges. However, a quantitative description regarding the coupling effect of the brace beams on the lateral resistance of an arch bridge is lacking.

As stated above, there is a strong need to further investigate the seismic mechanism of an RC arch bridge. A benchmark RC arch bridge, called the Heishuitan Bridge, was modeled with ABAQUS. The seismic performance of the Heishuitan Bridge was comprehensively investigated in the longitudinal and lateral direction. The sectional safety factor is proposed to quantitatively describe the mechanical status of the springing in the main arch under longitudinal excitation. Moreover, under lateral excitation, the coupling ratio (CR) is proposed as a non-dimensional coefficient that indicates the coupling effect between the arch ribs from the brace beams. To improve the lateral seismic performance, the further parametric analysis was carried out, the effects of the CR on the lateral seismic performance were verified, and the recommended CR was derived.

2. Seismic performance analysis

2.1. Benchmark RC arch bridge

The Heishuitan Bridge was employed as a benchmark bridge in the performance analysis described below. This bridge consists of three main parts; namely, two approach bridges with a length of 48 m and one main arch bridge with a length of 123.2 m. The main arch has a length of 120 m, the height of 24 m, and a rise-span ratio of 0.2. There are 21 portal frames placed on the main arch with a spacing of 5.6 m. In the approach bridge, the portal frames were designed with a spacing of

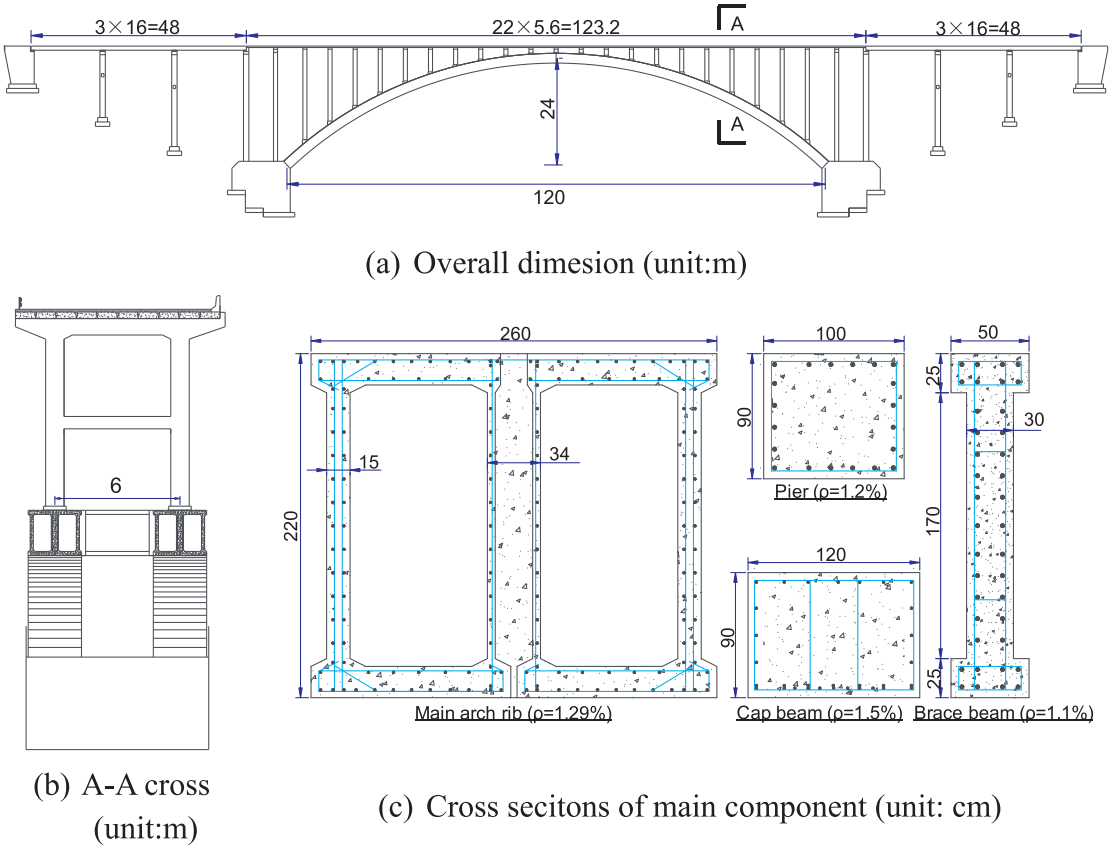

Fig. 1. Structure of benchmark RC arch bridge.

16 m. The second dead load on the main beam is 4.85 kN/m. The axial force ratio in the main arch is 0.37. The simply supported beams are used in the approach bridges and in the main arch span. The cross-sections of the arch ribs, portal frames on the arch ribs, piers, and beams in the bridge are also shown in Fig. 1. Two kinds of elastomeric pad bearings were adopted to support the beams at spans of 5.6 m and 16 m, respectively. In this bridge, C30 concrete and HRB335 rebar were used, and correspond to a nominal cubic compressive strength of 30 MPa and yielding tensile strength of 335 MPa, respectively.

This bridge is located in the Sichuan province, in China, and is approximately 100 km away from the central fault in the Longmen Mountain, which caused the 2008 Wenchuan earthquake. Prior to the Wenchuan earthquake, the earthquake fortification intensity in this area was 7°, and was in compliance with the Chinese seismic design code before the Wenchuan earthquake and corresponded to the peak ground motion acceleration (PGA) of 0.15 g for the design-based earthquake (DBE), and 0.255 g for the maximum considered earthquake (MCE). However, after the Wenchuan earthquake, the earthquake fortification intensity was improved, and the earthquake risk assessment report suggested a PGA of approximately 0.65 g in this area, which was considered as a very rare earthquake (VRE) intensity in the following analysis.

2.2. Modeling in ABAQUS

The finite element model was developed in ABAQUS, as shown in Fig. 2. B31 elements (3D Timoshenko beam elements) were used in the simulation of the arch ribs, brace beams, portal frames, and beams. The springing of the main arch ribs was fixed, as well as the pier bases in the portal frames in the approach bridge. The reinforcement was applied as sectional integration points. The dead load on the beam was introduced as the distribution weight on the beam elements. The constitutive models of the C30 concrete and HRB335 rebar are shown in the upper right corner in Fig. 2. The hysteretic model of the confined C30 concrete was derived following the suggestion of Mander [9], which considered the strength and stiffness degradation of concrete. The tensile stress of the concrete was neglected. The parameters of different RC components are listed in Table 1, which were suggested by the Chinese code for design of concrete structures [3]. The constitutive law of HRB335 rebar obeys the Clough constitutive model with the modified kinematic hardening. When subjected to the reversing loading, the stress-strain curve didn't directly point to the peak value (σ_{max}, ε_{max})in history, it pointed to the $0.2\sigma_{max}$ with the unloading stiffness. Then the strain-stress curve points to the peak value (σ_{max}, ε_{max}) in history [2] with reduced stiffness until achieving yielding stress. This model was very effective to reproduce the pinching effect in the reinforced concrete structure under large deformation. The post-yielding stiffness ratio of the HRB335 rebar was 0.01. When unloading to zero stresses, the reload path was evaluated towards the points with a maximum strain in the last loading cycle. In this model, the plasticity was introduced at the material level, and the coupled axial force and moment effect at the springing can be released.

Table 1
Material parameters for concrete in different components.

Component		Peak point		Ultimate point	
		Stress /MPa	Strain	Stress /MPa	Strain
Portal frame	Capping beam	21.8	2.9×10^{-3}	4.4	9.8×10^{-3}
	Brace beam	20.5	2.2×10^{-3}	4.1	10.6×10^{-3}
	Pier	21.4	2.7×10^{-3}	4.3	8.6×10^{-3}
Main arch	Arch rib	21.9	2.8×10^{-3}	4.4	7.7×10^{-3}
	Brace beam	20.8	2.3×10^{-3}	4.2	9.9×10^{-3}

The elastomeric pad bearings were simulated with the bi-linear connector. The initial shear stiffness K_0 and yielding capacity F_y of the connector were determined according to the design code for rubber bearing, as shown in Fig. 2 [10]. The post-yielding stiffness ratio was 0.1%. Several dummy rigid beams were used to connect the beams to the portal frames, as shown in the lower left corner in Fig. 2. In the actual bridge, there were eight elastomeric pad bearings supporting one end of the beams. In the numerical model, two equivalent nonlinear connectors were used to release the same overall stiffness and yielding strength. The nonlinear connectors were installed between the dummy rigid beams. Three transition degrees of the nonlinear connectors were available. The elastic-plastic properties were applied to the two shear directions, and the initial stiffness and yielding force are shown in

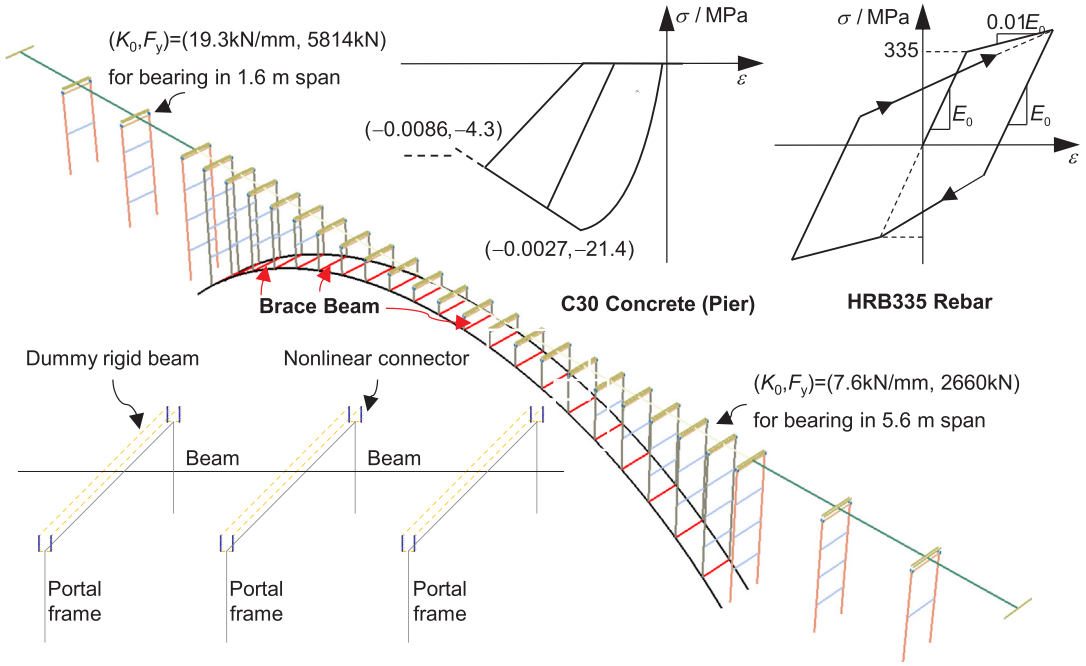

Fig. 2. Numerical model of RC arch bridge in ABAQUS.

Fig. 2. The only elastic properties were applied in the axial direction and were 3701 kN/mm for the 5.6 m span and 9438 kN/mm for the 16 m span. The rotation degrees of the nonlinear connectors were released. A damping ratio of 2% was applied to the model through Rayleigh damping, as shown in Eq. (1). The 1st and 3rd natural periods were used to derive the coefficients.

$$C = \alpha M + \beta K \Rightarrow \begin{cases} \alpha = \frac{2\delta\omega_1\omega_3}{\omega_1+\omega_3} \\ \beta = \frac{2\delta}{\omega_1+\omega_3} \end{cases} \quad (1)$$

Modal analysis was conducted based on the above model. The 1st to 20th vibration modes are listed in Table 2, and the main vibration modes are shown in Fig. 3. The first three modes are the fundamental modes in the lateral, longitudinal, and horizontal rotational directions, corresponding to the periods of 2.42 s, 1.45 s, and 1.29 s, respectively. The effective mass ratios of the fundamental modes in the longitudinal and lateral directions were larger than 50%. The main vertical modes appeared at the 14th and 17th modes, which had periods of 0.618 s and 0.571 s, corresponding to the effective mass ratios of 62.63% and 37.18%.

2.3. Earthquake record

The response spectra of the selected ground motions should be close to the design-based response spectra and correspond to the ground motion (GM) with a PGA of 0.15 g. Five GMs were selected in the NGA West 2 Ground Motion Database, which delivered the similar response spectra to the target design-based response spectrum. The mean squared error method was used to select the effective GMs. The period of interest ranged from 1.26 s (T_3) s to 2.37 s (T_1), and from 0.1 s to 0.45 s (characteristic site period) [5]. According to Fig. 4b, the mean response spectra of the five GMs fit well with the target response spectrum, particularly in the range of interest, which demonstrated the effectiveness of the selected GMs. In the nonlinear dynamic analysis, three typical earthquake intensities were considered, namely, DBE (PGA = 0.15 g), MCE (PGA = 0.255 g), and VRE (PGA = 0.65 g). The response spectrum of the GM3 had the largest value at the fundamental period of the bridge. Thus, the GM3 was selected as the representative GM, as will be discussed below.

3. Dynamic analysis results

3.1. Response under longitudinal excitation

The plastic hinge distributions under the GM3 at the DBE, MCE, and VRE intensities are shown in Fig. 5. The plastic hinge is defined as the yielding of the longitudinal reinforcement, and the compressive damage means that the confined concrete achieved its peak compressive strength, i.e., the concrete was crushed. At the DBE intensity, the plasticity was not obtained, whereas, at the MCE intensity, several plastic hinges appeared at the bottom of the piers and the springing. Moreover, the concrete did not incur compressive damage.

At the VRE intensity, several piers and the springing sustained compressive damage. Moreover, the compressive damage at the springing occurred at 18.5 s, without the advanced yielding of the reinforcement. This result is consistent with the field investigation regarding the Wenchuan earthquake, where moderate damage was rarely observed at the springing. The segments near the quarter-point and the springing sustained remarkable plasticity. This yielding distribution is the typically observed pattern for symmetrical arch bridge subjected to an anti-symmetric longitudinal earthquake effect.

The peak tensile and compressive strains of the springing sections are shown in Fig. 6, where ε_y is the yielding strain of the rebar, and ε_c and ε_u are the strain at the peak strength and at 20% peak strength of the C30 concrete. At the DBE intensity, the tensile strain did not appear at the springing section under GM5. However, GM2 excited the largest response, and the peak tensile strain reached up to 1.4×10^{-3}, which is smaller than ε_y. At the MCE and VRE intensities, the obviously large tensile strains indicated remarkable yielding at the springing. After such a strong earthquake, structural rehabilitation is necessary. Moreover, the peak compressive strains at the DBE and MCE intensities were almost the same and smaller than the strain corresponding to the peak compressive strength. The compressive damage did not occur. At the VRE intensity, the Heishuitan Bridge collapsed under the GM3 and the partial crushing at the springing occurred under GM2 and GM5, i.e., one or two corners of the springing section crushed.

The N-M interactions of the springing section under the GM3 are shown in Fig. 7. The sectional capacity was obtained by Xtract (TRC). The limiting conditions were 2.89×10^{-3} for the compressive strain of the C30 concrete and 1.67×10^{-3} for the strain of the HRB335 rebar. These results are consistent with the plastic hinge distribution. At the DBE intensity, plasticity did not occur. At the MCE intensity, the N-M interaction broke through the sectional capacity of the lower half, which indicated the yielding of the HRB335 rebar. At the VRE intensity, the N-M interaction broke the sectional capacity of the upper half, which indicated the crushing of the C30 concrete.

Based on the N-M interaction, the non-dimensional sectional safety factor η is proposed to describe the sectional performance. The definition of this factor is shown in Fig. 8a. For any point on the N-M interaction curve, such as the i^{th} point corresponding to the coordinate of (M_i, N_i), a straight line is drawn to connect this point to the initial point with coordinates (M_1, N_1), that is, the mechanical status under the gravity load. The nominal geometric distance between this point and the initial point was l_{1i}. l_{1i} was just a geometric intermediate variable, which didn't have actual physical meaning. Then, by extending this line in the direction from initial point to the i^{th} point, the intersection point between the extension line and the sectional capacity curve, corresponding to the coordinate of (M_{ci}, N_{ci}), can be found. If the i^{th} point is located out of the sectional capacity curve, the intersection point would be located between the i^{th} point and initial point, not on the extension line. The geometric distance between the intersection point and the initial point is l_{2i}. The entire N-M interaction curve is located within the sectional capacity curve, that is, l_{1i} is always smaller than l_{2i} for all points. Otherwise, if any point is located out of the sectional capacity curve, there must be one point, let us assume the j^{th} point, where l_{1j}/l_{2j} is larger than 1. Thus, the sectional safety factor η can be considered as the minimum value of $(1 - l_{1i}/l_{2i})$ traversing all the points on the N-M

Table 2
Eigenvalue analysis results of benchmark bridge.

Mode	Period (s)	Effective mass ratio			
		Longitudinal	Transverse	Vertical	Horizontal rotation
1	2.424	0.00%	**54.37%**	0.00%	0.00%
2	1.445	**92.38%**	0.00%	0.00%	0.18%
3	1.295	0.00%	0.00%	0.00%	0.00%
4	1.294	0.00%	0.00%	0.00%	**25.93%**
5	1.164	2.75%	0.00%	0.00%	0.00%
6	0.957	0.00%	**38.14%**	0.00%	0.00%
7	0.946	0.00%	0.00%	0.00%	**52.67%**
8	0.848	0.00%	0.35%	0.00%	0.00%
9	0.836	0.00%	0.00%	0.19%	0.00%
10	0.781	0.00%	0.00%	0.00%	8.05%
11	0.755	0.85%	0.00%	0.00%	0.00%
12	0.744	0.00%	4.98%	0.00%	0.00%
13	0.670	0.00%	0.00%	0.00%	8.43%
14	0.618	0.00%	0.00%	**62.63%**	0.00%
15	0.614	0.00%	1.75%	0.00%	0.00%
16	0.587	0.00%	0.00%	0.00%	4.66%
17	0.571	0.00%	0.00%	**37.18%**	0.00%
18	0.557	4.02%	0.00%	0.00%	0.00%
19	0.548	0.00%	0.40%	0.00%	0.00%
20	0.504	0.00%	0.00%	0.00%	0.05%

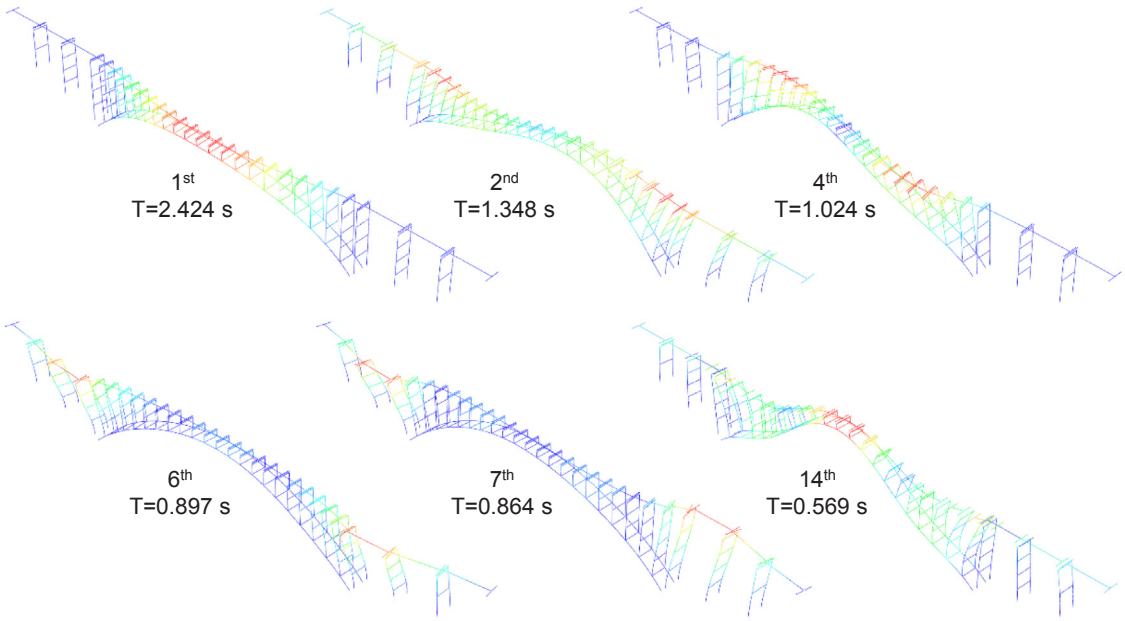

Fig. 3. Typical vibration modes of Heishuitan Bridge.

interaction curve, as expressed by Eq. (2). To this end, when there are some points located out of the N-M capacity curve, the sectional safety factor must be negative.

$$\eta = \min\left(1 - \frac{l_{1i}}{l_{2i}}\right) \tag{2}$$

Moreover, the greater absolute value of the negative η indicates a worse situation for the springing. Fig. 8b shows the statistics of η under all of the GMs at different earthquake intensities, and the mean values and standard deviations. At the DBE intensity, the mean value of the sectional safety factors was 0.189, which demonstrated the safety of the springing. At the MCE intensity, the mean value was approximately −0.093, with moderate damage at the MCE intensity. At the VRE intensity, all the section safety factors were negative, and the mean value was approximately −0.337. Moreover, the standard deviation of the section safety factors at the VRE intensity was quite small, which suggests the validity of the sectional safety factor.

3.2. Response under lateral excitation

The mid-span drifts are shown in Fig. 9. Under the GM3 at the VRE intensity, the mid-span drifts reached up to 3 m at 54.0 s, and soon completely collapsed. In total, two GMs caused the complete collapse at the VRE intensity. At the DBE and MCE intensities, the mean values of the peak drifts were approximately 0.35 m and 0.46 m respectively, which corresponded to the lateral drift ratios of 1.47% and 1.95%, with consideration to the span height of 24 m. At the VRE intensity, GM1 and GM3 caused the complete collapse of the RC arch bridge.

The plastic hinge distributions of the Heishuitan Bridge under the lateral GM3 excitation are shown in Fig. 10. At the DBE intensity, the conventional plastic hinge appeared at the pier base and the springing of the main arch, while at the MCE intensity, the more conventional plastic hinge and the compressive plastic hinge appeared at the springing of the main arch. At the VRE intensity, the RC arch bridge collapsed completely. The damage evolution was as follows: (1) tensile yielding in the brace beams and arch ribs; (2) compressive damage at the springing; (3) plastic hinge at mid-span. With three plastic hinges, the arch rib became a kinematic structure and soon collapsed at 54.0 s.

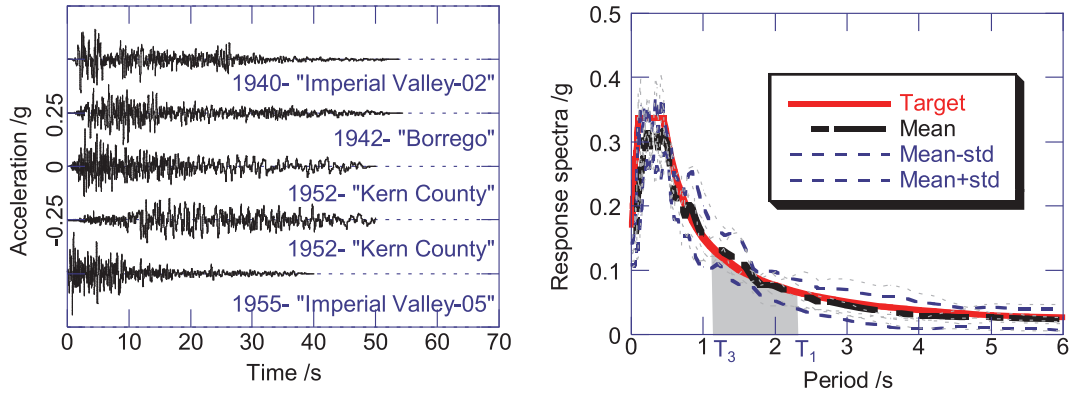

(a) Ground motion records (b) Response spectra

Fig. 4. Selected ground motions and response spectra.

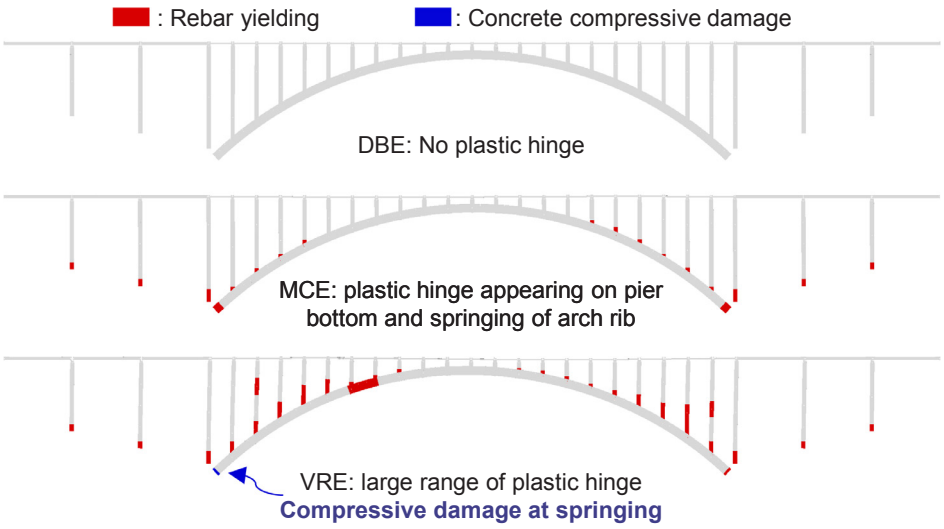

Fig. 5. Plastic hinge distribution under GM3 in longitudinal direction (scale factor: 1).

In comparison with the seismic performances under the longitudinal excitation, the lateral excitation caused much more serious earthquake damage to the Heishuitan Bridge.

Fig. 11 shows the peak strains at the springing sections. The tensile performance of the springing section was similar to the performance under the longitudinal excitation. However, observable compressive damages were incurred under the GM2 and GM3 at the MCE intensity. At VRE intensity, complete collapse occurred under GM2 and GM3. The results released the poor seismic performance in the lateral direction. Under lateral excitation, the arch bridge was subjected to 3-dimensional deformation, and the mechanical status of the springing was quite complex. The 3D stress state at the springing, axial force and bi-directional moments, caused remarkable difficulty for the selections of the lateral bending moment of inertia and reinforcement ratio. Moreover, the coupling effect exerted from the brace beams between the two arch ribs was not considered. Typically, the coupling effect can improve the lateral moment resistance

Fig. 12 presents the axial forces and lateral moments of the two arch springing at one side under the GM3 at the MCE intensity. The axial forces of the two arch ribs delivered a visible negative linear correlation, with a correlation coefficient of −0.58. This result indicates the coupled fluctuation of the axial forces in the two arch ribs. The moments in the two arch ribs presented the correlation coefficient of 0.99, which demonstrated the consistency of the moments at the springing of the two main arch ribs.

Based on the failure mode and sectional force, the mechanical schematic diagram of the main arch to resist the lateral load is shown in Fig. 11. This arch bridge resisted the lateral load mainly in two ways: the moment resistance of each arch rib and the coupling effect between the two ribs. Under the lateral load, each arch rib could provide its individual resistance, owing to the sectional bending strength. Moreover, the two arch ribs constitute the spacing frame through the brace beams. The coupling effect between the two arch ribs could also provide additional moment resistance.

Thus, when the arch ribs yielded, the balance equation for the main arch could be derived as Eq.(3), where *OM* is the overall moment at one end; M_{S1} (N_{S1}) and M_{S2} (N_{S2}) are the sectional moments (axial forces) at the springing of the two arch ribs respectively; M_{M1} and M_{M2} are the moments at the mid-span sections; l is the distance between the two arch ribs.

$$OM = M_{S1} + M_{S2} + M_{M1} + M_{M2} + (N_{S1} - N_{S2}) \times l \tag{3}$$

However, the difference between N_1 and N_2 originated from the shear capacity of the brace beams, as shown in the lower left of Fig. 11. Thus, Eq. (4) provides the formula to estimate the axial force difference after the brace beam yielded. In Eq. (4), F_i is the shear capacity of i^{th} brace beam and n is the number of the brace beams.

$$N_1 - N_2 = 2\sum_{i=1}^{[n/2]} F_i \tag{4}$$

Typically, the plastic hinges on the brace beams appear at the two ends. The shear capacity was obtained by Eq. (5), where m_i is the

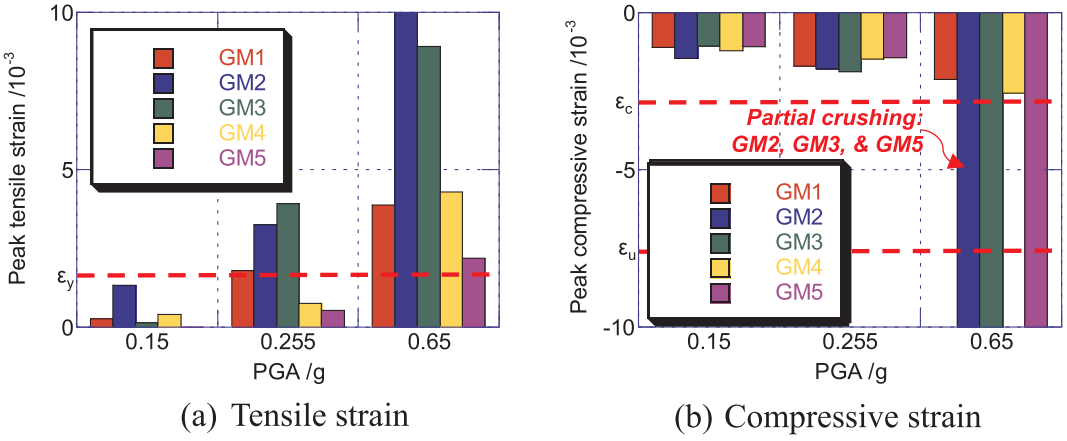

Fig. 6. Peak strains of springing section under longitudinal excitation.

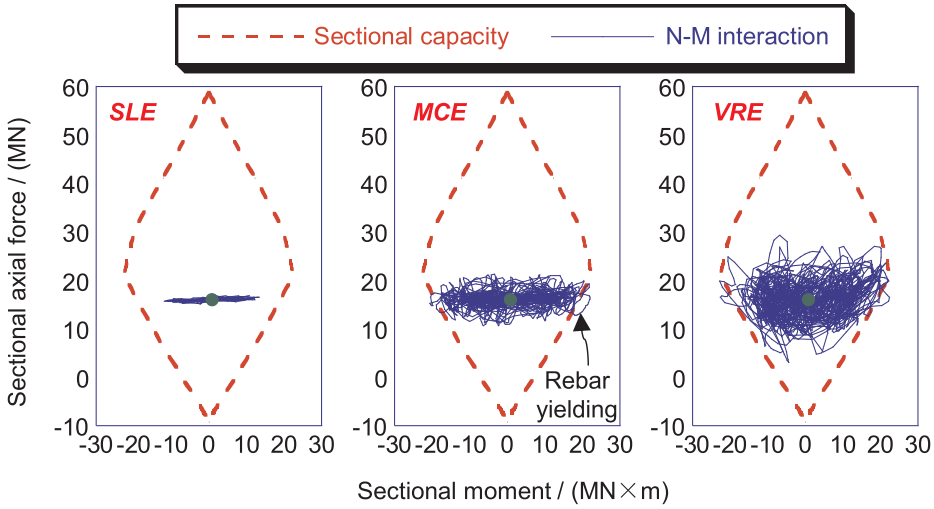

Fig. 7. N-M interaction of springing section under GM3.

sectional moment of the i^{th} brace beam and w is the width of the arch rib.

$$F_i = \frac{m_i}{l - w} \tag{5}$$

Note that the arch rib is a space curve in the earthquake, and brace beams may sustain bi-directional curvature, particularly with regard to the brace beams close to the springing. Fig. 13 shows a simplified approach towards estimating the sectional moment of the brace beam with consideration to the spacing effect. For each brace beam, it was assumed that the sectional neutral axis was perpendicular to the arch axis. Thus, the shear force of the brace beam could be transferred to the arch rib as its axial force. Moreover, according to the correlation coefficient, it was assumed that the M_{S1} was equal to M_{S2}, and M_{M1} was equal to M_{M2}. The arch rib has the same section along the entire length. Thus, the four moments could be considered as equal to the lateral yielding moment M_{sp}.

By substituting Eqs. (4) and (5) into Eq. (3), we obtain Eq. (6), where M is the yielding moment of the springing section in the lateral direction.

$$OM = 4M_{sp} + 2\sum_{i=1}^{[n/2]} \frac{m_i}{l - w} \times l \tag{6}$$

Based on the above discussion, a non-dimensional parameter called the coupling ratio (CR) is proposed as expressed by Eq. (7), which quantitatively describes the contribution of the coupling effect to the lateral moment resistance. Obviously, CR varies from 0 to 1.

$$CR = \frac{\sum_{i=1}^{[n/2]} \frac{m_i}{l - w} \times l}{2M_{sp} + \sum_{i=1}^{[n/2]} \frac{m_i}{l - w} \times l} \tag{7}$$

A different CR value would induce a different yielding mechanism, as shown in Fig. 14. When subjected to lateral deformation, the red and blue dots represent the possible plastic hinges, while the larger dots indicate more serious plastic evolutions. An excessively large CR, as shown in Fig. 14b, i.e., the over coupled effect, may comprise a tough space frame in the upper part of the main arch. Thus, four serious plastic hinges may occur at the bottom of the arch ribs, and the insufficient deformable length will result in serious plastic hinges in the arch ribs. Moreover, an excessively small CR, as shown in Fig. 14c, i.e., the under-coupled effect, could not provide an adequate coupling effect. When subjected to the lateral load, the main arch may deliver evident individual bending deformation, and two serious plastic hinges will form at the springing. Furthermore, there should be a balance between lateral deformability and load resistance. In summary, the brace beams should deliver the expected two-stage performance, that is, provide adequate lateral resistance under a small earthquake, and sufficient energy dissipation under a strong earthquake.

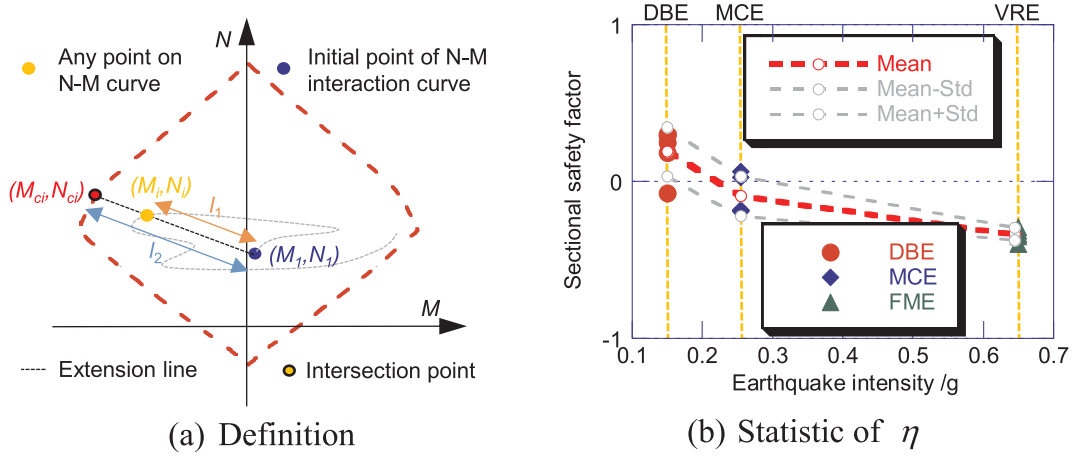

Fig. 8. Sectional safety factor analysis.

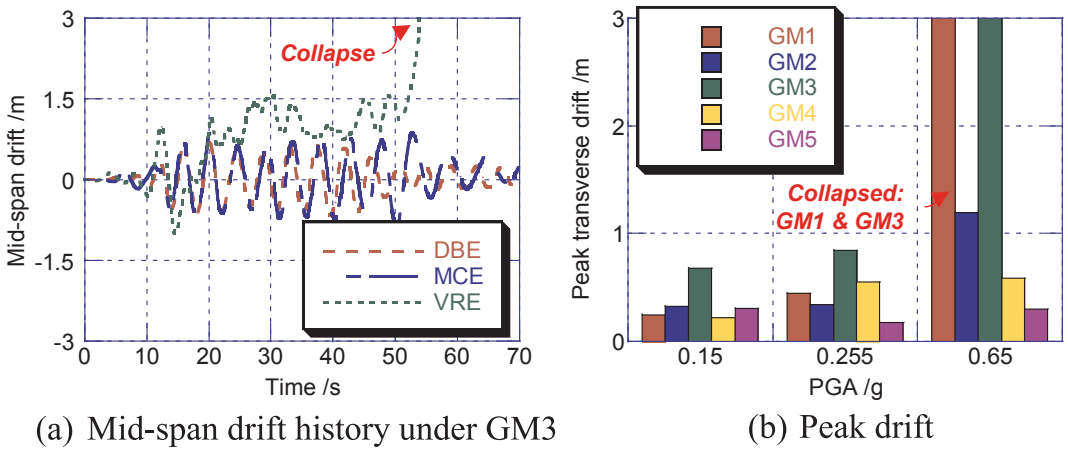

Fig. 9. Mid-span drift under lateral excitation.

4. Parametric analysis

According to this concept, the current design of the Heshuitan Bridge provides an original *CR* value of 0.27. For comparison, seven additional models with strengthened brace beams were analyzed, which corresponded to the *CRs* values of 0.37–0.75 with an approximate interval of 0.07. The sections of the brace beams in the new models are shown in Fig. 15. The original I-shaped section with a large aspect ratio is not suitable to the stable bearing and energy dissipation capacity; that is, it provides insufficient bearing capacity in the weak direction, and may not form the desired plastic hinges in the strong direction. To achieve the expected two-stage performance, the squared cross-sections were used in the strengthened brace beams and had the same reinforcement ratios as the original design.

Firstly, the modal analyses were conducted. The fundamental periods in lateral and longitudinal directions are shown in Fig. 16. The stronger brace beam led to the larger structural mass but didn't contribute to the longitudinal stiffness. Thus, the longitudinal period had a slight increase. On the other hand, with the increasing of *CR*, the fundamental period in lateral direction evidently reduced, which may increase the response of the arch bridge due to getting closer to the characteristic period of the ground motion. The optimal *CR* should be a balanced value between the enhancement of the capacity and reduction of the lateral period.

In the time history analysis, the same GMs were used in the parametric analysis. Note that, when *CRs* were larger than 0.41, no lateral collapse occurred at the VRE intensity. This result proved the effectiveness of enhancing the coupling effect with lateral collapse prevention.

The statistics of the peak lateral drifts at different intensities are shown in Fig. 17. For the collapsed case at the VRE intensity, the mid-span peak lateral drifts were assumed to be 5 m. At the DBE, MEC and VRE intensities, the maximum mid-span drifts decreased quickly when CR increased from 0.27 to 0.48. From weak coupling effect to moderate coupling effect, the period of the arch bridge decreased, owing to the strong brace beam, and resulted in the reduction of the lateral deformation. At the MCE and VRE intensities, the stronger brace beams with squared sections could provide better energy dissipation. However, further increase of CR led to the slight increase of the maximum mid-span drift. As addressed above, the reduction in natural period may intensify the energy input to the arch bridge, and amplify the seismic response.

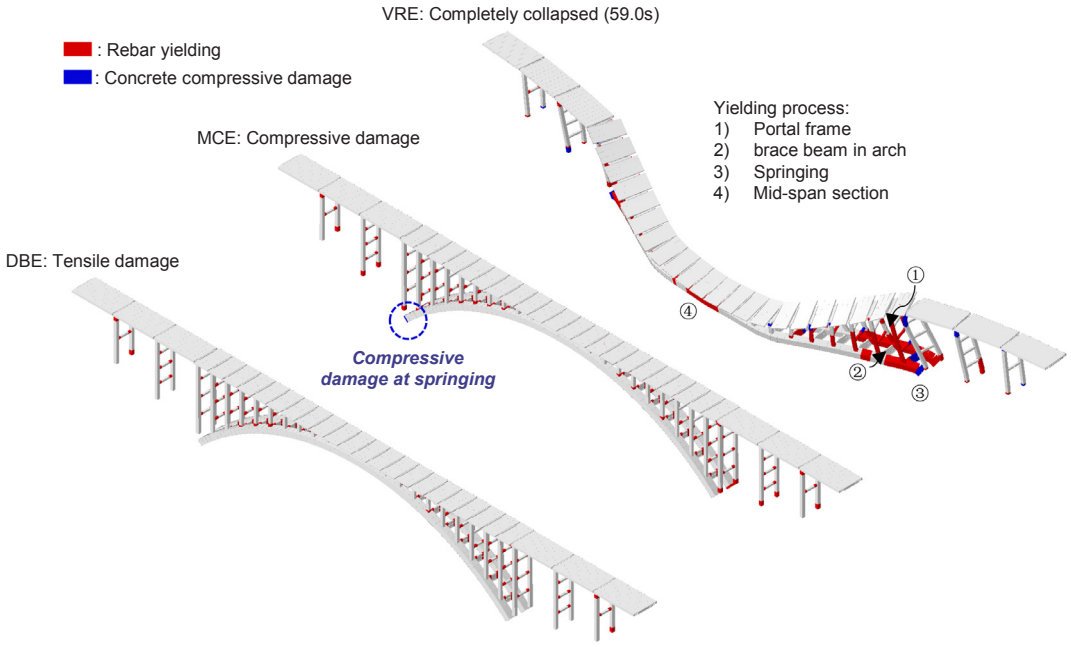

Fig. 10. Plastic hinge distribution under GM3 in lateral direction (Scale Factor: 1).

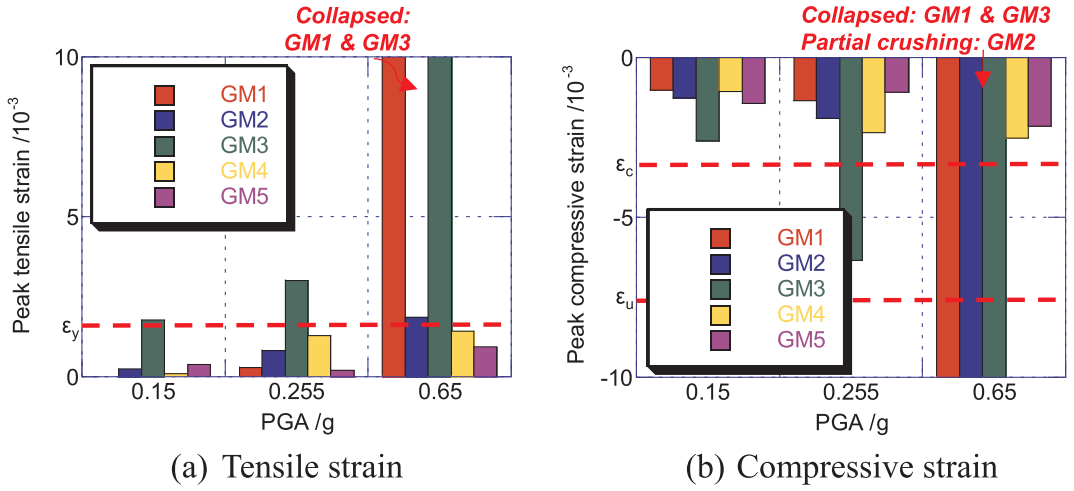

Fig. 11. Peak strains of springing section under lateral excitation.

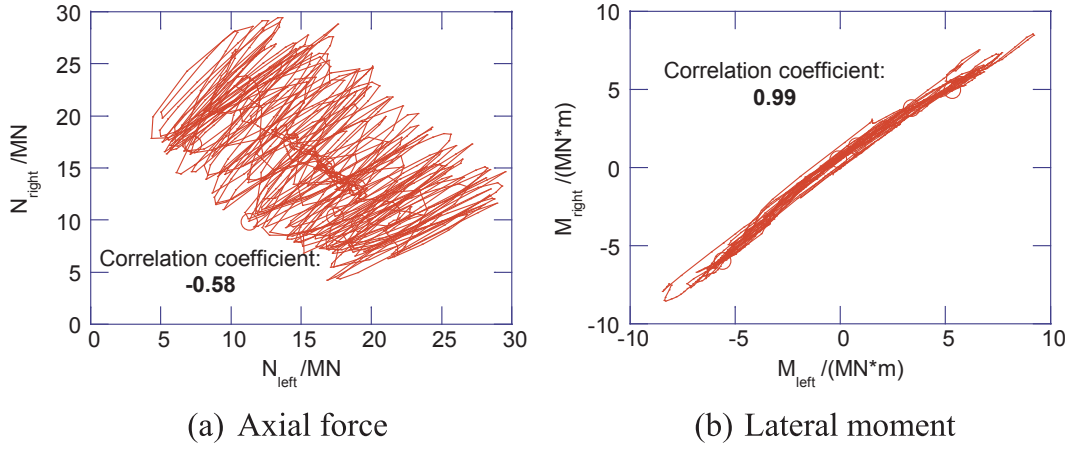

Fig. 12. Comparison of N-M statuses of springing under GM3 at MCE intensity.

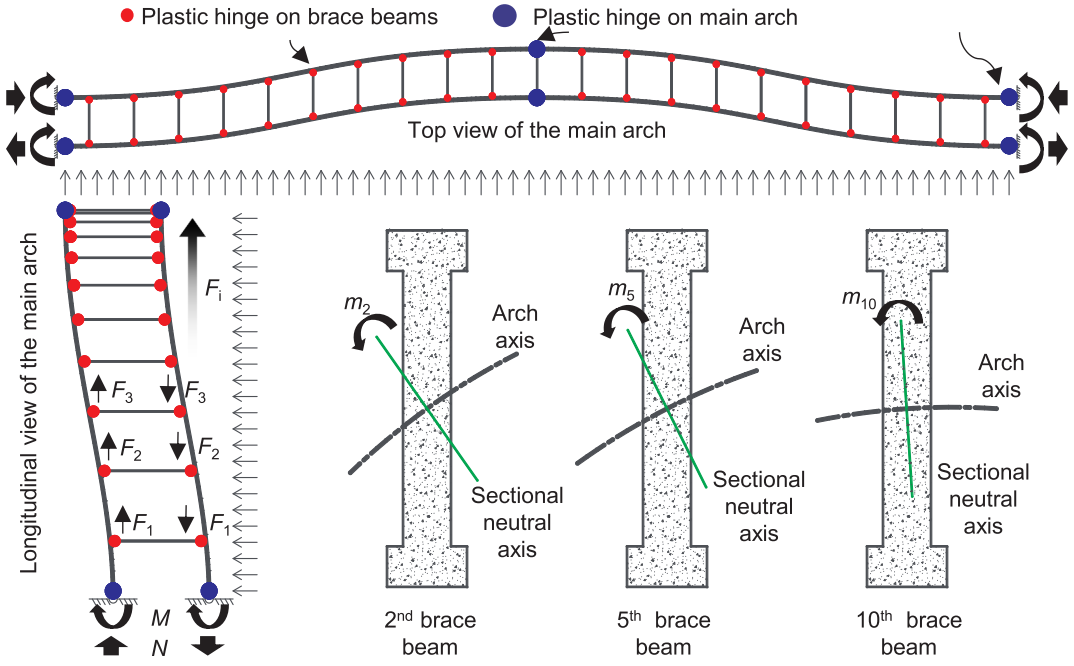

Fig. 13. Damage mechanism of RC arch bridge in lateral direction.

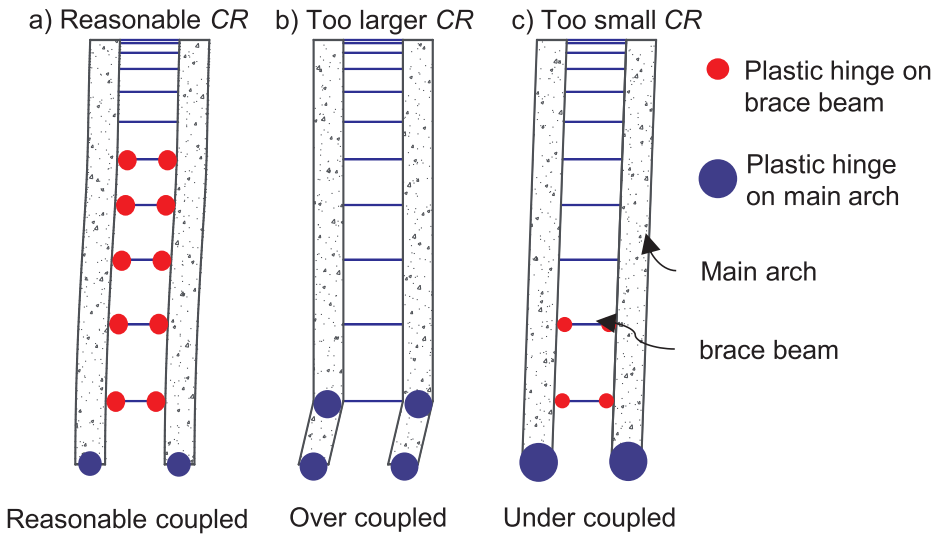

Fig. 14. Coupling mechanism of arch bridge with different *CR* (unit: cm).

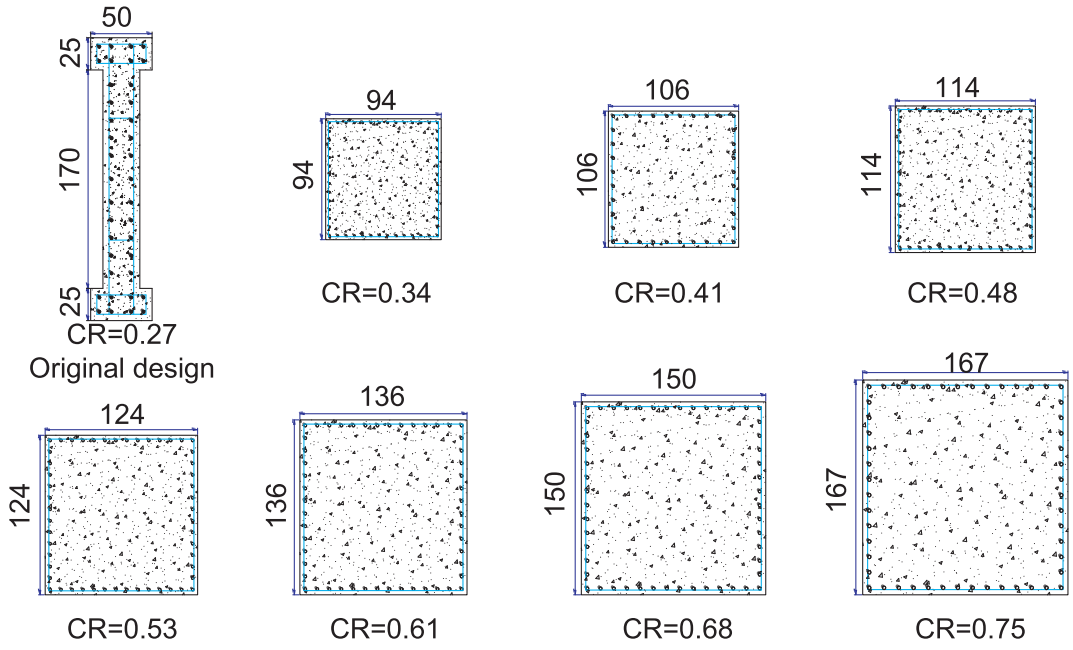

Fig. 15. Strengthened brace beams corresponding to larger *CRs* (ρ = 1.1%).

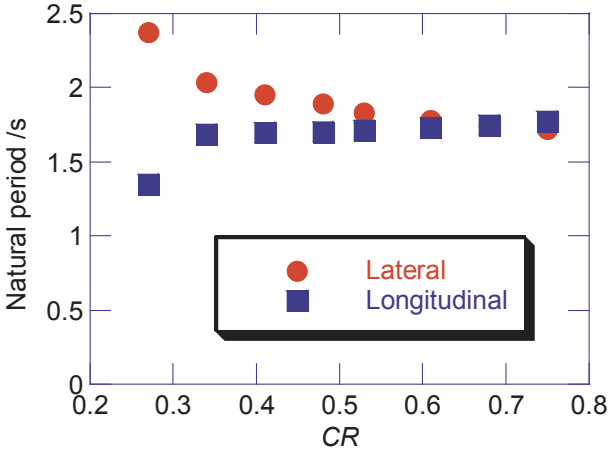

Fig. 16. Natural period of 1st lateral vibration mode.

Fig. 18 shows a comparison of the peak compressive strain at the springing in the bridges with different *CR*. At the VRE intensity, the partial crushing of the concrete occurred at the springing, and the peak compressive strains were excessively large. The quantitative statistics were meaningless. Thus, only the DBE results and the MCE intensities are discussed. The peak compressive strain presented the same laws with the maximum mid-span drift. Compared with weak small *CR*, the larger *CR* could enhance the coupling effect between the two arch ribs. Thus, the individual bending deformation at each springing was adequately controlled, and the maximum compressive strain was significantly decreased. On the other hand, an excessively strong brace beam may restrain the deformation of the arch and provide poor energy dissipation capacity. The over coupling effect introduced visible additional constraint to the main arch ribs and resulted in the reduction of effective length at the springing. As a comprehensive consideration of the mid-span drift and strain of the springing, a *CR* value of 0.41 with a squared cross section is recommended for the Heishuitan Bridge.

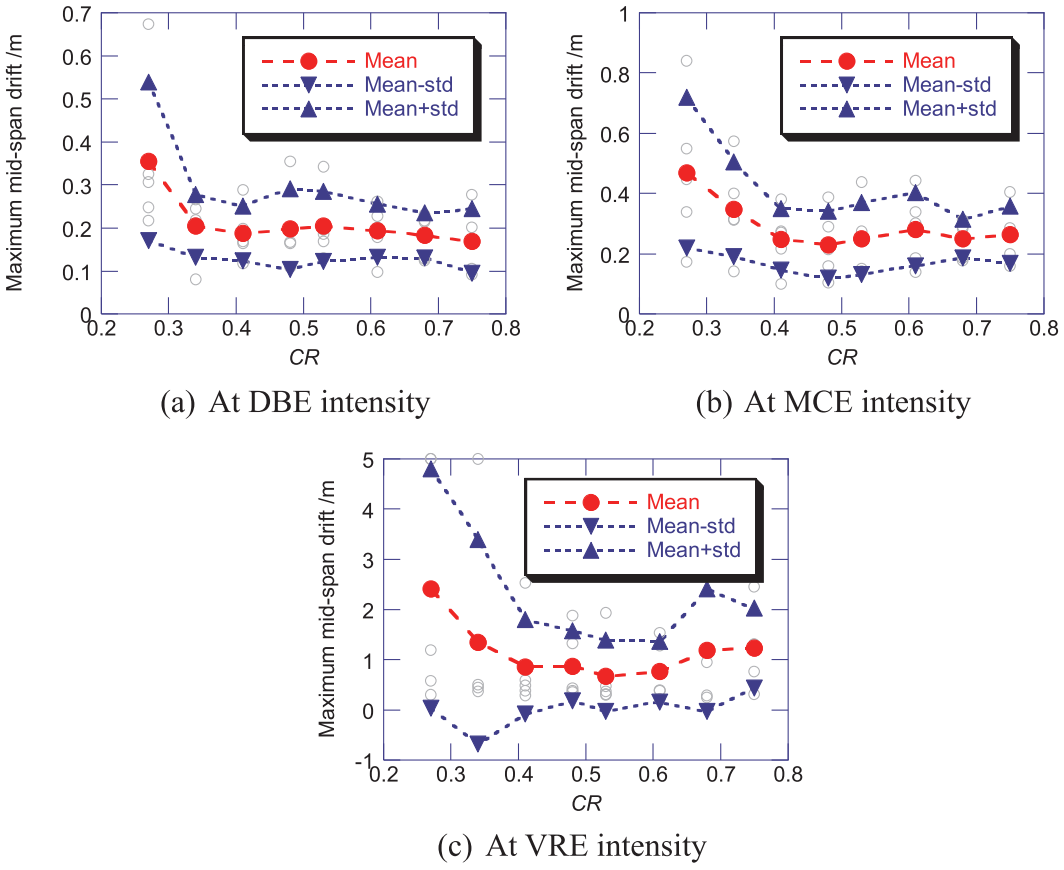

Fig. 17. Effect on peak mid-span drift under lateral excitation.

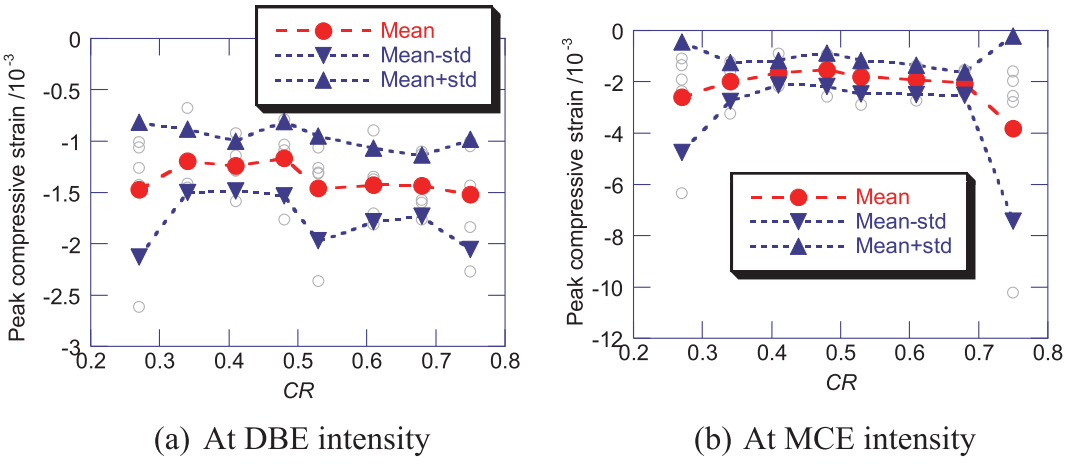

Fig. 18. Effect of *CR* on peak compressive strain at springing.

5. Conclusion

This paper presented a comprehensive investigation into the seismic performance of a benchmark reinforced concrete (RC) arch bridge. The longitudinal and lateral seismic performances were discussed in depth. The sectional safety factor was proposed to quantitatively describe the damage degree of the springing under longitudinal excitation. Moreover, under lateral excitation, the RC arch bridge sustained unacceptable damages. The coupling ratio (*CR*) was developed as a non-dimensional coefficient to account for the contribution of the brace beams to the moment resistance. Further parametric investigations were conducted to obtain the recommended *CR*. The major conclusions drawn from this study are as follows:

(1) Under longitudinal excitation at the VRE intensity, the compressive damage of the concrete confined at the springing occurred without advanced yielding, which explains the extreme nature of the earthquake damage in RC arch bridges;
(2) The proposed section safety factor could quantitatively describe the damage degree of the springing in the RC arch bridge, and exhibited a remarkable consistency with the strain development and N-M interaction under longitudinal excitation;
(3) The brace beams exerted a significant influence on the lateral seismic performance, and a non-dimensional coefficient called *CR* was proposed to quantitatively calculate the contribution from the brace beams;
(4) Employing large brace beams may reduce the fundamental period

of lateral vibration modes, which may be closer to the characteristic period of the ground motions. The recommended *CR* should be a balanced value between the enhancement of the capacity and reduction of the lateral period.

(5) According to the parametric analysis, an excessively large or small *CR* may unexpectedly trigger the yielding mechanism of the arch bridge. A value of 0.41 was proposed for the considered benchmark RC arch bridge because it delivered better damage control performance.

Acknowledgment

This study was under the support of the National Natural Science Foundation of China (Grant No. 51708466), the Fundamental Research Funds for the Central Universities (Grant No. 2682017CX002), and the research plan of Shanghai Railway Bureau (2018145). We also really appreciate the support from Hefei Special Material Technology Co., Ltd.

References

[1] Alvarez JJ, Aparicio AC, Jara JM, Jara M. Seismic assessment of long-span arch bridge considering the variation in axial forces induced by earthquakes. Eng Struct 2012;34:69–80.
[2] Gao X, Zhang Y. Nonlinear analysis of a RC column under cycling loads. Struct Eng 2013;30(3):56–63.
[3] Chinese Ministry of Housing and Urban Rural Development. Code for design of concrete structures GB50010-2010. China Architecture and Building Press; 2013.
[4] Han Q, Du X, Liu J, Li Z, Li L, Zhao J. Seismic damage of highway bridges during the 2008 Wenchuan earthquake. Earthquake Eng Eng Vib 2009;8(2):263–73.
[5] Ji X, Liu D, Sun Y, Molina Hutt C. Seismic performance assessment of a hybrid coupled wall system with replaceable steel coupling beams versus traditional RC coupling beams. Earthquake Eng Struct Dyn 2017;46(4):517–35.
[6] Khan E, Sullivan TJ, Kowalsky MJ. Direct displacement–based seismic design of reinforced concrete arch bridges. J Bridge Eng 2013;19(1):44–58.
[7] Li J, Peng T, Xu Y. Damage investigation of girder bridges under the Wenchuan earthquake and corresponding seismic design recommendations. Earthquake Eng Eng Vib 2008;7(4):337–44.
[8] Lu Z, Ge H, Usami T. Applicability of pushover analysis-based seismic performance evaluation procedure for steel arch bridges. Eng Struct 2004;26(13):1957–77.
[9] Mander JB, Priestley MJ, Park R. Theoretical stress-strain model for confined concrete. J Struct Eng 1988;114(8):1804–26.
[10] Ministry of Transport of the People's Republic of China. Series of elastomeric pad bearings for highway bridges. Shandong Science and Technology Press; 2006. (In Chinese).
[11] Morcous G, Hanna K, Deng Y, Tadros MK. Concrete-filled steel tubular tied arch bridge system: application to Columbus viaduct. J Bridge Eng 2010;17(1):107–16.
[12] Modena C, Tecchio G, Pellegrino C, da Porto F, Donà M, Zampieri P, et al. Reinforced concrete and masonry arch bridges in seismic areas: typical deficiencies and retrofitting strategies. Struct Infrastruct Eng 2015;11(4):415–42.
[13] Sakai J, Kawashima K. Seismic response of a reinforced concrete arch bridge taking account of axial force and moment interaction. Doboku Gakkai Ronbunshu 2003;2003(724):69–81. (In Japanese).
[14] Usami T, Lu Z, Ge H. A seismic upgrading method for steel arch bridges using buckling-restrained braces. Earthquake Eng Struct Dyn 2005;34(4–5):471–96.
[15] Wang KH, Sun YH, Wer H, Li Q, Jiang ZY. Comments on seismic strengthening for structural engineering in China after Wenchuan earthquake. J Highway Transp Res Dev 2008;25(11):54–9. (In Chinese).
[16] Zanardo G, Pellegrino C, Bobisut C, Modena C. Performance evaluation of short span reinforced concrete arch bridges. J Bridge Eng 2004;9(5):424–34.